Next-to-leading order QCD corrections to a heavy resonance production and decay into top quark pair at the LHC

Jun Gao, Chong Sheng Li,* Bo Hua Li, and Hua Xing Zhu

Department of Physics and State Key Laboratory of Nuclear Physics and Technology, Peking University, Beijing 100871, China

C.-P. Yuan†

Department of Physics and Astronomy, Michigan State University, East Lansing, 48824, USA

We present a complete next-to-leading order (NLO) QCD calculation to a heavy resonance production and decay into a top quark pair at the LHC, where the resonance could be either a Randall-Sundrum Kaluza-Klein graviton G or an extra gauge boson Z'. The complete NLO QCD corrections can enhance the total cross sections by about 80%–100% and 20%–40% for the G and the Z', respectively, depending on the resonance mass. We also explore in detail the NLO corrections to the polar angle distributions of the top quark, and our results show that the shapes of the NLO distributions can be different from the leading order ones for the Kaluza-Klein graviton. Moreover, we study the NLO corrections to the spin correlations of the top quark pair production via the above process, and find that the corrections are small.

I. INTRODUCTION

The top quark is the heaviest particle so far discovered, with a mass close to the electroweak symmetry breaking scale, and closely related to various new physics models beyond the standard model (SM). Thus, it provides an effective probe for the electroweak symmetry breaking mechanism and the new physics beyond the SM through studying its production and decay at colliders. The Large Hadron Collider (LHC) is running now with a center of mass energy $\sqrt{s} = 7$ TeV, and will collect 1 fb^{-1} experimental data during the initial run. After this initial state the LHC will turn to $\sqrt{s} = 14$ TeV, with a design luminosity of ~ 10 fb^{-1}/yr there will be 8×10^6 top quark pairs and 3×10^6 single top quarks produced yearly. As a result of all these, the precision measurement of the top quark properties, such as the mass, the production cross sections, the kinematic distributions, and the spin correlation effects, will be one of the prime tasks in the experiments at the LHC, and any deviations from the SM predictions will definitely be a hint for new physics beyond the SM.

To explore the connections between the new physics and the top quark, one possibility is to study the top quark pair invariant mass distribution and look for possible resonances since many new physics models predict the existence of a new resonance with a mass around TeV, which can decay into a top quark pair, such as the Technicolor [1], Topcolor [2], Little Higgs [3], general Z' models [4,5], and Randall-Sundrum (RS) models [6]. In addition, in many such models the interaction between the heavy resonance and the top quark is enhanced as compared to the other fermions and the resonance will mainly decay into a top

quark pair, for example, the Kaluza-Klein (KK) excitations of the graviton [7], the gluon [8] as well as the weak gauge bosons [9] in the extended RS models. Once we have discovered such a resonance in the top quark pair invariant mass distribution, the next step is to measure its spin and couplings, and finally determine the underlying new physics dynamics, which have been studied in Refs. [10,11]. It has been suggested in Refs. [10,11] that it is possible to extract the spin and coupling information of the resonance from the top quark polar angle distributions and the spin correlations of the top quark pair. Those studies were carried out at the leading order (LO) in QCD interactions. However, the next-to-leading order (NLO) QCD corrections may be large, for example, the NLO QCD corrections can enhance the cross sections of the single RS KK graviton or the Z' production by about 70% [12,13] and 20% [14], respectively, so it is necessary to examine whether the QCD corrections will change the tree-level results and some conclusions of Refs. [10,11] or not. In this paper we investigate the NLO QCD effects to a heavy resonance production and decay into a top quark pair, i.e., $pp \rightarrow X(\text{color singlet}) \rightarrow t\bar{t}$, at the LHC, where the $SU(3)_C$ color singlet state X could be either a RS KK graviton G or an extra gauge boson Z'.

The arrangement of this paper is as follows. Section II is a brief review to the relevant models. In Sec. III we show the details of the NLO calculations. Section IV contains the numerical results, and Sec. V is a brief summary. The Appendix collects some analytic results at the LO.

II. THE MODELS

A. The RS KK graviton

In the RS model, a single extra dimension is compactified on a S^1/Z_2 orbifold with a radius r, which is not too

---

*csli@pku.edu.cn
†yuan@pa.msu.edu

large as compared to the Planck length. Two 3-branes, the Planck brane and the TeV brane, are located at the orbifold fixed points $\phi = 0$, π, respectively, and the spacetime between the two 3-branes is simply a slice of a five-dimensional anti–de Sitter geometry. The five-dimensional warped metric is given by

$$ds^2 = e^{-2kr|\phi|}\eta_{\mu\nu}dx^\mu dx^\nu - r^2 d\phi^2, \quad (1)$$

where ϕ is the five-dimensional coordinate, and $k \sim M_P$ is the curvature scale. By requiring $kr \sim 12$, one can suppress the Planck scale to $M_P e^{-k\pi r} \sim O$ (TeV) on the TeV brane, and then solve the gauge hierarchy problem. The gravity fields are treated as fluctuations under the background metric, and after expanding the gravity fields in the extra dimension we get infinite massive KK gravitons, which can interact with the SM fields [15].

The RS KK graviton can be produced through both the gg fusion and the $q\bar{q}$ annihilation at the LO as shown in Fig. 1. The detailed Feynman rules of the graviton couplings can be found in Ref. [16], and the propagator of the graviton in the unitary gauge in n dimensions is given by [12]

$$P_G(k) = \frac{iB_{\mu\nu,\rho\sigma}(k)}{k^2 - m_X^2 + im_X\Gamma_X}, \quad (2)$$

with

$$B_{\mu\nu,\rho\sigma}(k) = \left(g_{\mu\rho} - \frac{k_\mu k_\rho}{m_X^2}\right)\left(g_{\nu\sigma} - \frac{k_\nu k_\sigma}{m_X^2}\right)$$
$$+ \left(g_{\mu\sigma} - \frac{k_\mu k_\sigma}{m_X^2}\right)\left(g_{\nu\rho} - \frac{k_\nu k_\rho}{m_X^2}\right)$$
$$- \frac{2}{n-1}\left(g_{\mu\nu} - \frac{k_\mu k_\nu}{m_X^2}\right)\left(g_{\rho\sigma} - \frac{k_\rho k_\sigma}{m_X^2}\right), \quad (3)$$

where m_X and Γ_X are the mass and the width of the heavy resonance, respectively.

B. The extra gauge boson Z'

The extra gauge boson Z' could arise from an additional $U(1)'$ gauge symmetry [4]. It could also be the KK excitation of the electroweak gauge bosons. It can only be produced through the $q\bar{q}$ annihilation at the LO, and its generic couplings to quarks are as follows:

$$Z'q\bar{q} \sim \gamma_\mu\left(a_L\frac{1-\gamma_5}{2} + a_R\frac{1+\gamma_5}{2}\right). \quad (4)$$

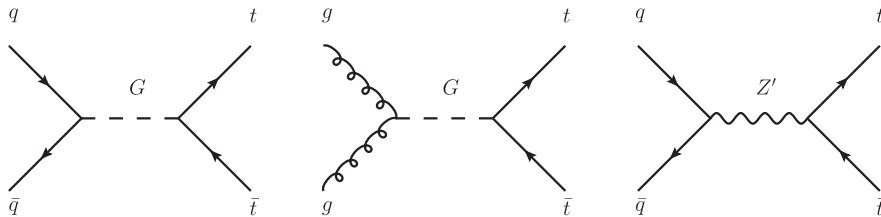We considered four combinations of a_L and a_R, i.e., the pure vector coupling, $a_L = a_R = 1$, the axial-vector coupling, $a_L = -a_R = -1$, the right-handed coupling, $a_L = 0$, $a_R = 1$, and the left-handed coupling, $a_L = 1$, $a_R = 0$, which are denoted by Z'_1, Z'_2, Z'_3, and Z'_4, respectively. The propagator of the Z' in the unitary gauge is given by

$$P_{Z'}(k) = \frac{i}{k^2 - m_X^2 + im_X\Gamma_X}\left(-g_{\mu\nu} + \frac{k_\mu k_\nu}{m_X^2}\right). \quad (5)$$

In our calculations of the process $pp \rightarrow X(\text{color singlet}) \rightarrow t\bar{t}$, what we are mainly concerned about are the ratios of the NLO results to the LO ones, so it is not necessary to specify the actual values of all the couplings. We simply assume the mass of the heavy resonance to be around TeV scale, which is not yet excluded by the current experiments. Besides, we only consider the narrow resonance cases and fixes $\Gamma_X/m_X = 1\%$ at both the LO and the NLO. We do not expect our conclusions to be largely modified even if Γ_X/m_X increases to be at the order of 10%. Detailed discussions on the SM backgrounds and the discovery potential of the process can be found in Refs. [10,11].

III. THE NLO FORMALISM

The complete NLO QCD corrections to the process $pp \rightarrow X(\text{color singlet}) \rightarrow t\bar{t}$ can be factorized into two independent gauge invariant parts, i.e., the heavy resonance produced at the NLO with a subsequent decay at the LO, and produced at the LO with a subsequent decay at the NLO, similar to the cases studied in Ref. [17]. The box diagrams, and the corresponding real correction diagrams that connect the initial and the final states do not contribute to the squared matrix elements up to the NLO as the heavy resonance is a $SU(3)_C$ color singlet particle. This whole procedure can be illustrated as follows:

$$|\mathcal{M}_{2\rightarrow 2}^{\text{tree}}|^2 = |\mathcal{M}_{\text{pro}}^{\text{tree}}|^2 \otimes |\mathcal{M}_{\text{dec}}^{\text{tree}}|^2 \otimes |P_X|^2,$$
$$|\mathcal{M}_{2\rightarrow 3}^{\text{real}}|^2 = \{|\mathcal{M}_{\text{pro}}^{\text{tree}}|^2 \otimes |\mathcal{M}_{\text{dec}}^{\text{real}}|^2$$
$$+ |\mathcal{M}_{\text{pro}}^{\text{real}}|^2 \otimes |\mathcal{M}_{\text{dec}}^{\text{tree}}|^2\} \otimes |P_X|^2, \quad (6)$$
$$\mathcal{M}_{2\rightarrow 2}^{\text{tree*}}\mathcal{M}_{2\rightarrow 2}^{\text{loop}} = \{|\mathcal{M}_{\text{pro}}^{\text{tree}}|^2 \otimes (\mathcal{M}_{\text{dec}}^{\text{tree*}}\mathcal{M}_{\text{dec}}^{\text{loop}})$$
$$+ |\mathcal{M}_{\text{dec}}^{\text{tree}}|^2 \otimes (\mathcal{M}_{\text{pro}}^{\text{tree*}}\mathcal{M}_{\text{pro}}^{\text{loop}})\} \otimes |P_X|^2,$$

we have suppressed the possible Lorentz indices here for simplicity.

FIG. 1. Tree-level Feynman diagrams for the heavy resonance production and decay into a top quark pair.
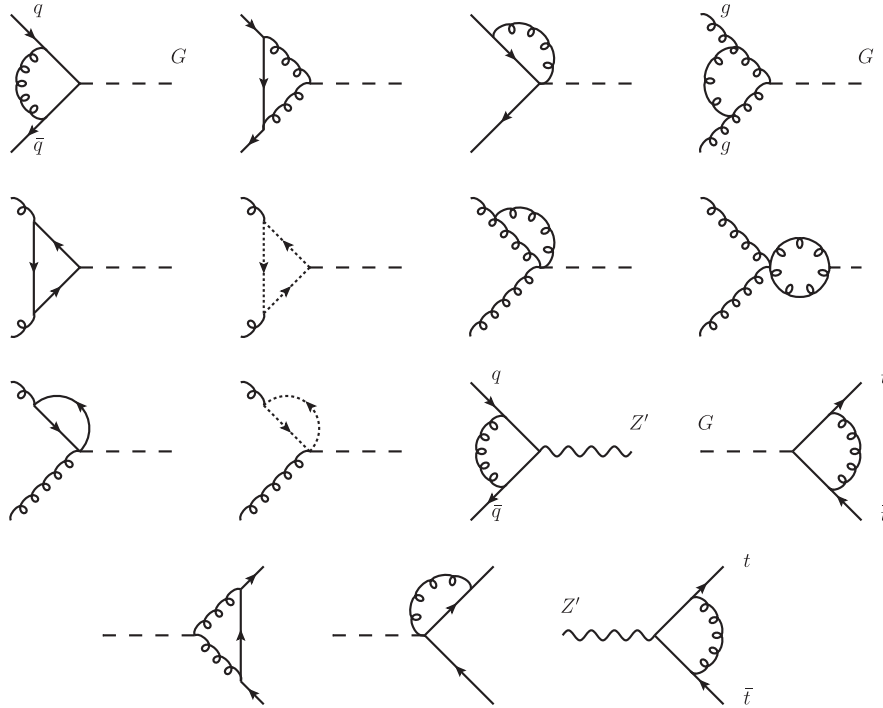
FIG. 2.   Some one-loop Feynman diagrams for the production and the decay of the heavy resonances. Others not shown can be obtained by the exchange of the external quark or gluon lines.

We calculate the full squared matrix elements using the propagators (P_X) of the heavy resonance given in Sec. II, which can incorporate the full spin correlations between the production and decay processes in order to generate the correct kinematic distributions. We carry out all the QCD calculations in the 't Hooft-Feynman gauge and use the dimension regularization scheme [18] (with the naive γ_5 prescription [19]) in $n = 4 - 2\epsilon$ dimensions to regularize

all the divergences. The one-loop Feynman diagrams for the production and the decay of the heavy resonance are shown in Fig. 2.

Figure 3 shows the real correction Feynman diagrams for the production and the decay of the heavy resonance. The infrared divergences of the real corrections are extracted by using the two cutoff phase space slicing method
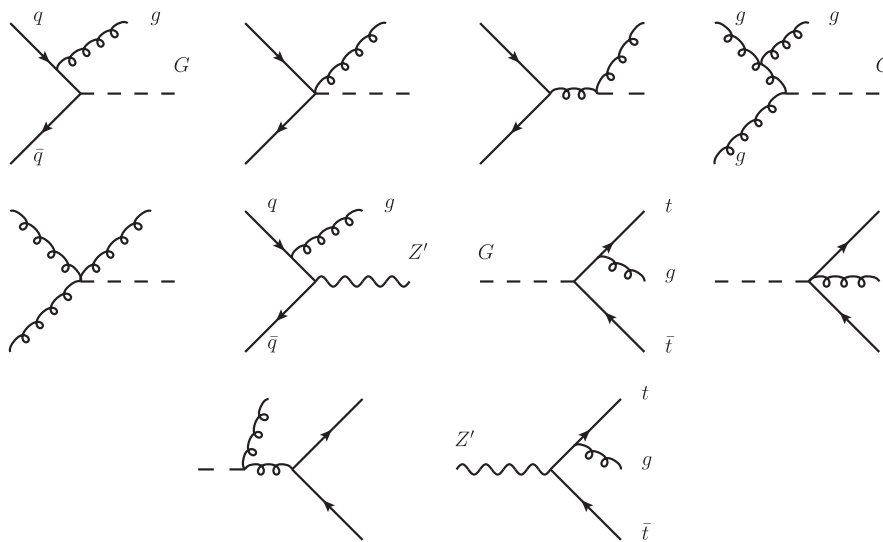

FIG. 3.   Some real correction Feynman diagrams for the production and the decay of the heavy resonances. Others not shown can be obtained by the exchange of the external quark or gluon lines.

[20]. Because of the limited space here we do not reproduce the details of the method.

IV. NUMERICAL RESULTS

In our numerical calculations we choose the input parameters to be $m_{\text{top}} = 171$ GeV, $m_Z = 91.188$ GeV, and $\alpha_s(m_Z) = 0.118$ [21]. The running QCD coupling constant is evaluated at the three-loop order [21] with $n_f = 5$, and the CTEQ6M (CTEQ6L1) parton distribution function (PDF) set [22] is used through the NLO (LO) calculations. We set both the renormalization and factorization scales equal to the mass of the heavy resonance, unless specified. Besides, in the two cutoff phase slicing method there are two arbitrary cutoff parameters, i.e., the soft cutoff δ_s and the collinear cutoff δ_c. We have checked the cutoff dependence of all our numerical results, and found that the dependence is negligibly small for $\delta_s \leq 1 \times 10^{-3}$, so we choose $\delta_s = 1 \times 10^{-3}$ and $\delta_c = \delta_s/50$ to obtain the numerical results presented below.

A. The total cross sections

In Fig. 4 we show the NLO K factor, defined as the ratio of the NLO cross section σ_{NLO} to the LO cross section σ_{LO}, as a function of the heavy resonance mass at the LHC with different center of mass energies. We can see that the total NLO QCD corrections can be large, which can enhance the total cross sections by about 80%–100% and 20%–40% for the G and all four types of Z' bosons, respectively, depending on the resonance mass. The NLO corrections from the production part are dominant, while the ones from the decay part are relatively small, but can still reach above ten percent in some regions. Our results of the NLO K factors of the production part agree with the ones given in Refs. [13,14], where the total cross sections have been summed over the spins of the heavy resonance directly. In the following parts of our paper we will only

show the results of the total NLO QCD corrections for simplicity. We further present the ratios of the total cross sections from the different channels for the graviton at both the LO and the NLO in Fig. 5. It can be seen that the contribution from the gg channel is dominant at the low m_X value region due to the large PDF of the gluon, and the contribution from the $q\bar{q}$ channel becomes important at the high m_X value region since the PDF of the valence quark decreases more slowly than the gluon. And the NLO corrections can change the ratio of the contribution from the $q\bar{q}$ channel to the one from the gg channel significantly.

B. The polar angle and invariant mass distributions

It has been shown in Refs. [10,11] that the polar angle distributions of the top quark are the key points to extract the spin and coupling information of the heavy resonance. The definition of this polar angle depends on the reference frame and axis chosen, here we considered two kinds of polar angles, one is the Collins-Soper angle θ_S [23], which is defined to be the angle between the top quark momentum and the axis that bisects the angle between the momentums of the incoming hadrons ($\vec{p}_A$ and $-\vec{p}_B$) in the $t\bar{t}$ rest frame, and for the Z' we can define θ^* as the angle in the $t\bar{t}$ rest frame between the top quark momentum and the incident quark momentum which can be determined by the longitudinal boost direction of the $t\bar{t}$ rest frame at the LHC [10].

In Figs. 6–8 we show the normalized polar angle distributions of the top quark at the LO and the ratios of the normalized NLO distributions to the LO ones at the LHC with $\sqrt{s} = 14$ TeV. At the LO, we can use both the $\cos\theta_S$ and $\cos\theta^*$ distributions to distinguish the Z' and the G as their distributions have significantly different shapes. At the same time we can also use the $\cos\theta^*$ distribution to distinguish between the $Z'_{1,2}$ and the $Z'_{3,4}$ since the latter ones have a large forward-backward asymmetry. Furthermore, the differences of the polar angle distributions between the Z'_1 and the Z'_2 are very small for m_X around
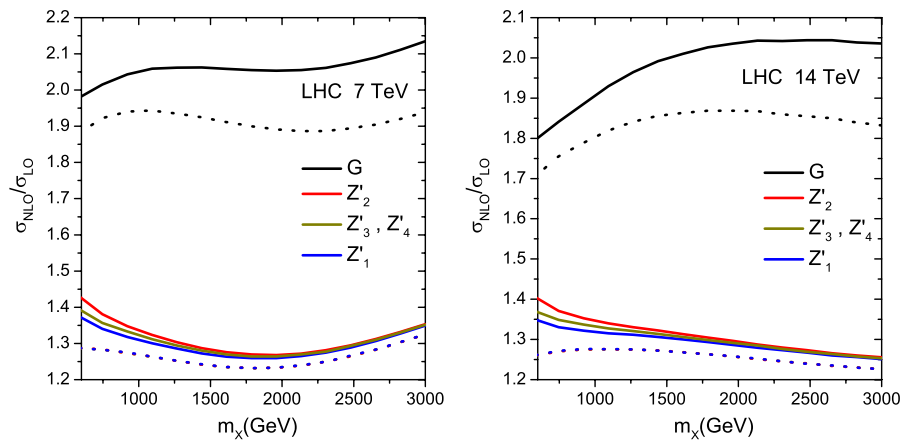

FIG. 4 (color online). The NLO K factors as functions of the heavy resonance mass at the LHC. The solid and dotted lines correspond to including the total NLO QCD corrections and the corrections from the production part alone, respectively. The four groups of the curves from the top to the bottom correspond to the G, Z'_2, $Z'_3(Z'_4)$, and Z'_1, respectively.
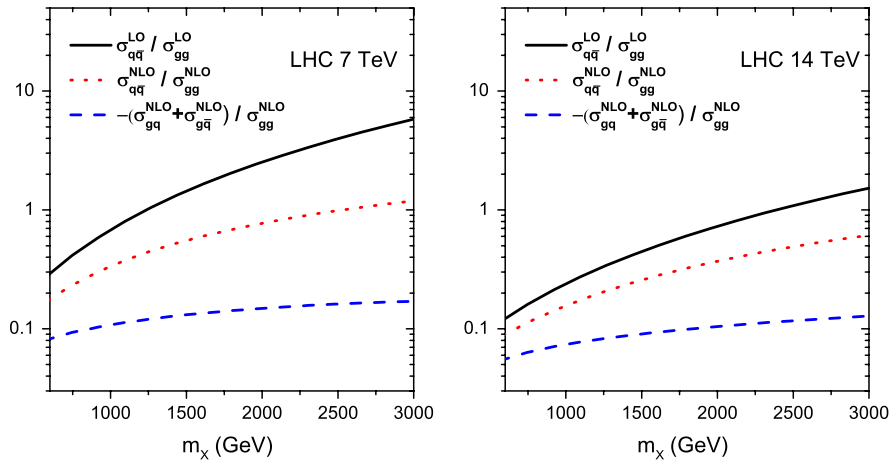
FIG. 5 (color online).　The ratios of the total cross sections from different channels for the graviton as functions of the graviton mass at both the LO and the NLO.
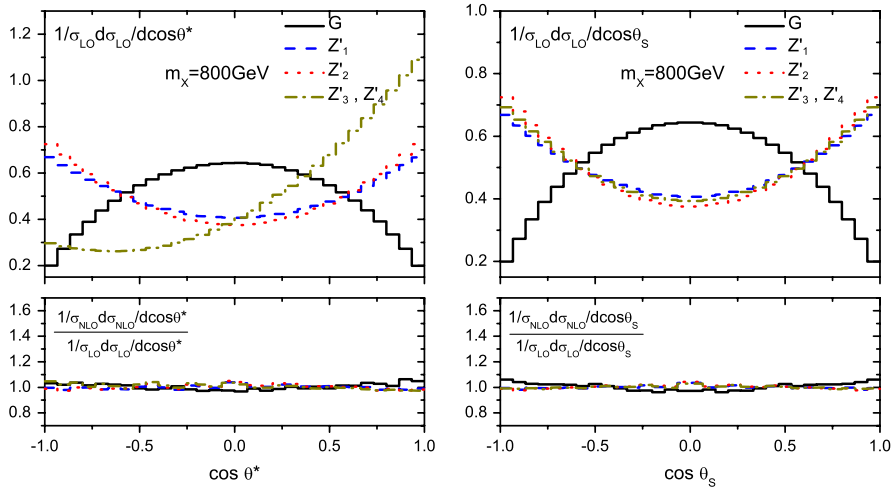

FIG. 6 (color online).　The normalized top quark polar angle distributions at the LO and the ratios of the normalized NLO distributions to the LO ones, at the LHC with $\sqrt{s} = 14$ TeV for $m_X = 800$ GeV.

FIG. 7 (color online).　The normalized top quark polar angle distributions at the LO and the ratios of the normalized NLO distributions to the LO ones, at the LHC with $\sqrt{s} = 14$ TeV for $m_X = 1500$ GeV.
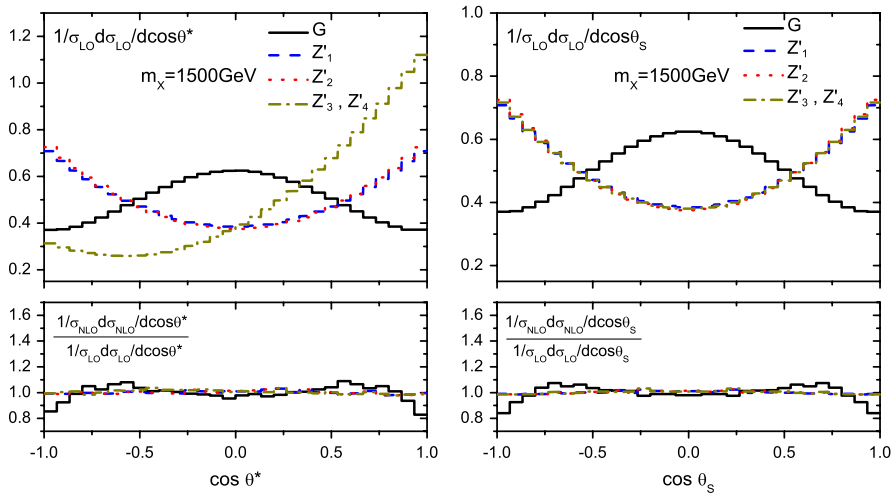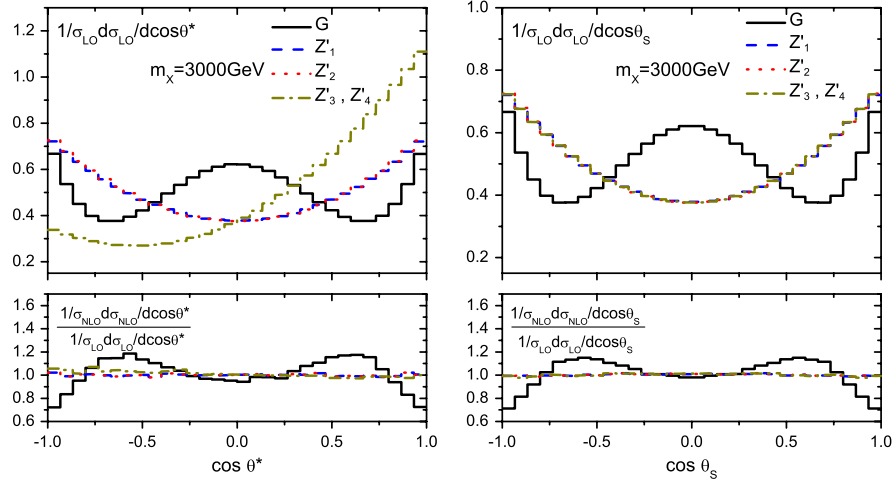
FIG. 8 (color online). The normalized top quark polar angle distributions at the LO and the ratios of the normalized NLO distributions to the LO ones, at the LHC with $\sqrt{s} = 14$ TeV for $m_X = 3000$ GeV.

1 TeV or heavier, thus it is not possible to separate them through the polar angle distributions. We present the LO squared helicity amplitudes in the Appendix, which can explain the behavior of the LO polar angle distributions. After including the NLO corrections, we can see that for all the Z' the changes of the distributions are negligibly small, which are no more then a few percent. But for the G, as the increasing of the resonance mass the NLO corrections can change the shapes of the distributions, for example, the NLO corrections make the distributions decrease more quickly at the both ends and can reach about 10% for $m_X = 1500$ GeV. The corrections can be as large as 30%, and change the shapes of the distributions significantly for $m_X = 3000$ GeV, which do not change the fact that the distributions of the G and the Z' are greatly different. Note that for a heavy enough resonance, the top quarks produced are highly boosted, which means the decay products of the

top quark are close to each other and form a top jet. Recently, several methods based on the jet substructures have been proposed [24], which may be used to detect such a top jet efficiently, so it is possible to measure the NLO QCD effects to the polar angle distributions for a graviton with a mass of several TeV at the LHC. The reason that the NLO distributions for the graviton differ from the LO ones is that the NLO corrections change the ratio of the contributions from the gg and $q\bar{q}$ channels, as shown in Sec. IV A, which have different shapes of distributions. As the resonance mass increases, the contributions from these two channels become comparable, so the changes are more significant. We further study the scale and PDF uncertainties of the NLO polar angle distributions for a graviton with $m_X = 3000$ GeV. As shown in Fig. 9, the uncertainty from the scale dependence is negligibly small, and the PDF uncertainty is within 10%, which is still small
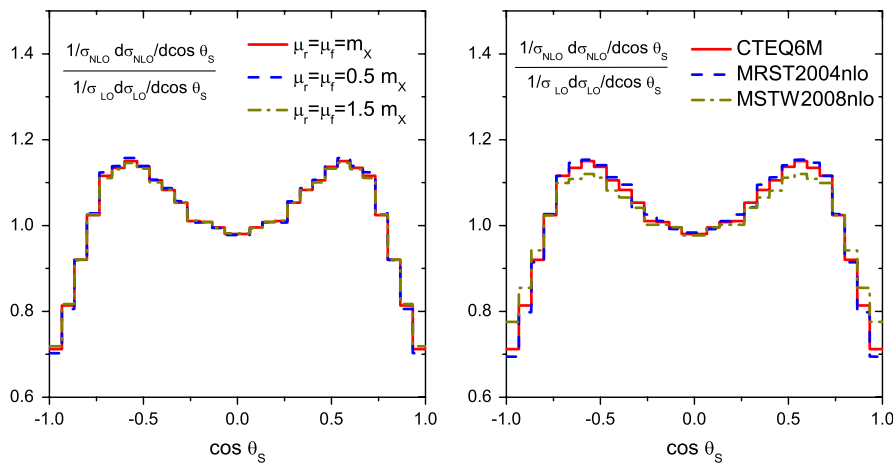

FIG. 9 (color online). The scale and PDF uncertainties of the NLO polar angle distribution for the graviton at the LHC with $\sqrt{s} = 14$ TeV and $m_X = 3000$ GeV.
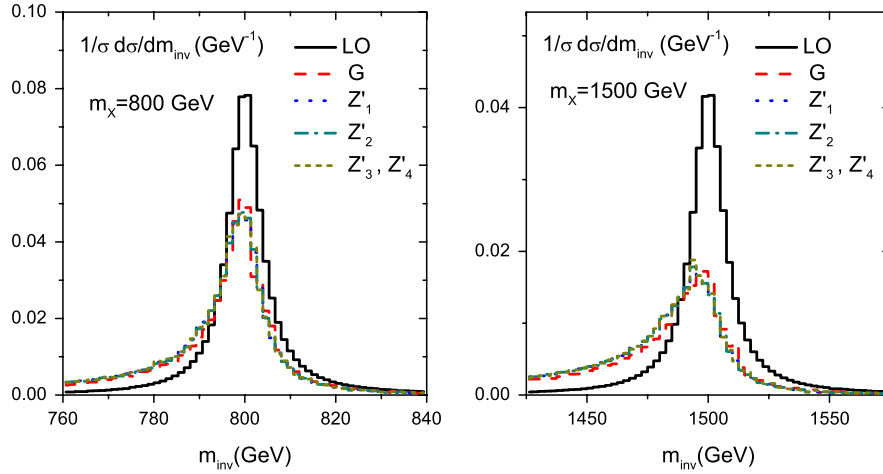
FIG. 10 (color online).   The normalized top quark pair invariant mass distributions at both the LO and the NLO at the LHC with $\sqrt{s} = 14$ TeV The solid line corresponds to the LO result, and the other lines correspond to the NLO ones.

as compared to the NLO corrections. Here, we use two more PDF sets in the NLO calculations, i.e., the MRST2004nlo [25] and MSTW2008nlo [26] PDF sets.

In Fig. 10 we present the invariant mass distributions of the top quark pair including the NLO QCD corrections. At the LO they are just the Breit-Wigner distributions with a center value m_X and a width Γ_X. While at the NLO the heavy resonance can decay into a top quark pair plus a hard gluon, so the NLO corrections increase the distributions in the lower invariant mass value region, and the changes of the distributions are more significant as the resonance mass increases. We also studied all the above distributions at the LHC with $\sqrt{s} = 7$ TeV, and the results are similar.

C. The spin correlations

One of the unique features of the top quark is that it decays before the strong interaction can depolarize its spin. Thus, it is possible to extract the spin information of the produced top quark by studying the angular distributions of the decay products. For a spin up top quark (or a spin down anti-top quark), the decay angular distribution of the i-th decay product is given by [27]

$$\frac{1}{\Gamma_T} \frac{d\Gamma}{d(\cos\chi_i)} = \frac{1}{2}(1 + \alpha_i \cos\chi_i), \tag{7}$$

where i could be quarks, b, u, c, $\bar{d}$, $\bar{s}$, or leptons, ν_l, $\bar{l}$; χ_i is the angle between the i-th decay product and the spin quantization axis in the top rest frame, and α_i are the correlation coefficients. For the charged leptons, $\alpha_l = 1$ exactly, which means the charged leptons are maximally correlated with the top spin direction.

The spin correlations of the top quark pair also can be used for the identification of the heavy resonance, but the precision measurement of them is more difficult at the LHC. In order to study the spin correlations of the top quark pair production, the following double differential

cross section is usually considered:

$$\frac{1}{\sigma} \frac{d^2\sigma}{d(\cos\chi_i^+)d(\cos\chi_j^-)} = \frac{1}{4}(1 - A\alpha_i\alpha_j \cos\chi_i^+ \cos\chi_j^-$$
$$+ b_+\alpha_i \cos\chi_i^+ + b_-\alpha_j \cos\chi_j^-), \tag{8}$$

neglecting the interference between the top spins we have

$$A = \frac{\sigma(t_\uparrow \bar{t}_\uparrow + t_\downarrow \bar{t}_\downarrow) - \sigma(t_\uparrow \bar{t}_\downarrow + t_\downarrow \bar{t}_\uparrow)}{\sigma(t_\uparrow \bar{t}_\uparrow + t_\downarrow \bar{t}_\downarrow) + \sigma(t_\uparrow \bar{t}_\downarrow + t_\downarrow \bar{t}_\uparrow)},$$
$$b_+ = \frac{\sigma(t_\uparrow \bar{t}_\uparrow + t_\uparrow \bar{t}_\downarrow) - \sigma(t_\downarrow \bar{t}_\uparrow + t_\downarrow \bar{t}_\downarrow)}{\sigma(t_\uparrow \bar{t}_\uparrow + t_\downarrow \bar{t}_\downarrow) + \sigma(t_\uparrow \bar{t}_\downarrow + t_\downarrow \bar{t}_\uparrow)}, \tag{9}$$
$$b_- = \frac{\sigma(t_\uparrow \bar{t}_\downarrow + t_\downarrow \bar{t}_\downarrow) - \sigma(t_\uparrow \bar{t}_\uparrow + t_\downarrow \bar{t}_\uparrow)}{\sigma(t_\uparrow \bar{t}_\uparrow + t_\downarrow \bar{t}_\downarrow) + \sigma(t_\uparrow \bar{t}_\downarrow + t_\downarrow \bar{t}_\uparrow)}.$$

In our following calculations we use the helicity basis in the $t\bar{t}$ center of mass frame, which means $\chi_i^+(\chi_j^-)$ is defined to be the angle between the $t(\bar{t})$ direction in the $t\bar{t}$ center of mass frame and the corresponding decay product direction in the $t(\bar{t})$ rest frame.

In Fig. 11 we show the LO results of the top quark pair spin correlation coefficients as functions of the heavy resonance mass at the LHC with $\sqrt{s} = 14$ TeV. According to symmetry analysis we have

$$A(Z_3') = A(Z_4'), \qquad b_\pm(G, Z_1', Z_2') = 0,$$
$$b_+(Z_3') = b_-(Z_3') = -b_+(Z_4') = -b_-(Z_4'), \tag{10}$$

and at the LO for the axial vector Z_2',

$$A(Z_2') = -1, \tag{11}$$

which can be seen from the helicity amplitudes in the Appendix. With the increasing heavy resonance mass, all the coefficients in Fig. 11 approach -1 due to the fact that the cross sections for the $t\bar{t}$ with the same helicities vanish
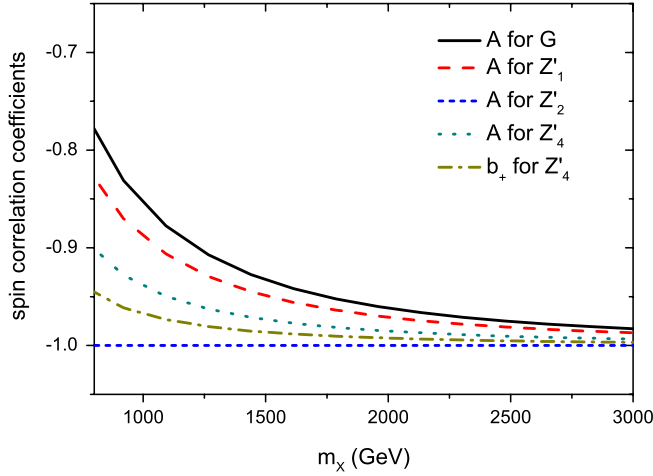
FIG. 11 (color online). The top quark pair spin correlation coefficients at the LO as functions of the heavy resonance mass at the LHC with $\sqrt{s} = 14$ TeV.

as the heavy resonance mass goes to infinity. In Table I, we list some typical NLO results of those coefficients. We can see that the NLO QCD corrections are rather small, about 1%–2%, and can be neglected at the LHC. We also investigate the cases for $\sqrt{s} = 7$ TeV, and the results are almost the same at both the LO and the NLO.

V. CONCLUSIONS

We have calculated the complete NLO QCD corrections to a heavy resonance production and decay into a top quark pair at the LHC, where the resonance could be either a RS KK graviton G or an extra gauge boson Z'. Our results

show that the total NLO K factors can reach about 1.8–2.0 and 1.2–1.4 for the G and all four types of Z' bosons, respectively, depending on the resonance mass. And the NLO corrections from the production part are dominant, while the ones from the decay part are relatively small but can still reach above ten percent in some parameter regions. We also explore in detail the NLO corrections to the polar angle distributions of the top quark, and our results show that the NLO distributions are almost the same as the LO ones for all four types of Z' bosons, while the shapes of the NLO distributions can be significantly different from the LO ones for the G, depending on the mass of the resonance. Moreover, the NLO corrections can also change the shapes of the top quark pair invariant mass distributions. Finally, we study the NLO corrections to the spin correlations of the top quark pair, and find that the corrections are negligibly small.

APPENDIX

In this appendix we give the individual nonvanishing LO squared helicity amplitudes for a heavy resonance production and decay into a top quark pair, $q\bar{q}(gg) \to X \to t\bar{t}$. For all the Z' mediated processes,

$$\overline{|\mathcal{M}|^2}_{Z'_1} = \begin{cases} (1 - \beta^2)\sin^2(\theta)\mathcal{A}, & \text{for helicities } \{+-++\}, \{+---\}, \{-+++\}, \text{ and } \{-+--\} \\ 4\sin^4(\theta/2)\mathcal{A}, & \text{for helicities } \{+--+\} \text{ and } \{-++-\} \\ 4\cos^4(\theta/2)\mathcal{A}, & \text{for helicities } \{+-+-\} \text{ and } \{-+-+\} \end{cases} \tag{A1}$$

$$\overline{|\mathcal{M}|^2}_{Z'_2} = \begin{cases} 4\beta^2\sin^4(\theta/2)\mathcal{A}, & \text{for helicities } \{+--+\} \text{ and } \{-++-\} \\ 4\beta^2\cos^4(\theta/2)\mathcal{A}, & \text{for helicities } \{+-+-\} \text{ and } \{-+-+\} \end{cases} \tag{A2}$$

TABLE I. The top quark pair spin correlation results at the LHC with $\sqrt{s} = 14$ TeV.

Mass (GeV)	resonance	A (LO)	A (NLO)	b_+ (LO)	b_+ (NLO)	b_- (LO)	b_- (NLO)
800	G	-0.783	-0.778	0	0	0	0
	Z'_1	-0.832	-0.826	0	0	0	0
	Z'_2	-1.000	-0.986	0	0	0	0
	Z'_3	-0.904	-0.896	0.947	0.943	0.947	0.943
	Z'_4	-0.904	-0.896	-0.947	-0.943	-0.947	-0.943
1500	G	-0.933	-0.913	0	0	0	0
	Z'_1	-0.949	-0.933	0	0	0	0
	Z'_2	-1.000	-0.980	0	0	0	0
	Z'_3	-0.974	-0.955	0.986	0.977	0.986	0.977
	Z'_4	-0.974	-0.955	-0.986	-0.977	-0.986	-0.977

$$\overline{|\mathcal{M}|^2}_{Z'_3} = \begin{cases} (1 - \beta^2)\sin^2(\theta)\mathcal{A}/4, & \text{for helicities } \{+ - + +\} \text{ and } \{+ - - -\} \\ (1 - \beta)^2\sin^4(\theta/2)\mathcal{A}, & \text{for helicities } \{+ - - +\} \\ (1 + \beta)^2\cos^4(\theta/2)\mathcal{A}, & \text{for helicities } \{+ - + -\} \end{cases}, \tag{A3}$$

$$\overline{|\mathcal{M}|^2}_{Z'_4} = \begin{cases} (1 - \beta^2)\sin^2(\theta)\mathcal{A}/4, & \text{for helicities } \{- + + +\} \text{ and } \{- + - -\} \\ (1 - \beta)^2\sin^4(\theta/2)\mathcal{A}, & \text{for helicities } \{- + + -\} \\ (1 + \beta)^2\cos^4(\theta/2)\mathcal{A}, & \text{for helicities } \{- + - +\} \end{cases}, \tag{A4}$$

and for the graviton mediated processes through the $q\bar{q}$ annihilation and the gg fusion,

$$\overline{|\mathcal{M}|^2}_{G,q\bar{q}} = \begin{cases} \beta^2(1 - \beta^2)\sin^2(2\theta)\mathcal{B}/64, & \text{for helicities } \{+ - + +\}, \{+ - - -\}, \{- + + +\}, \text{ and } \{- + - -\} \\ \beta^2(1 + 2\cos(\theta))^2\sin^4(\theta/2)\mathcal{B}/16, & \text{for helicities } \{+ - - +\} \text{ and } \{- + + -\} \\ \beta^2(1 - 2\cos(\theta))^2\cos^4(\theta/2)\mathcal{B}/16, & \text{for helicities } \{+ - + -\} \text{ and } \{- + - +\} \end{cases}, \tag{A5}$$

$$\overline{|\mathcal{M}|^2}_{G,gg} = \begin{cases} 3\beta^2(1 - \beta^2)\sin^4(\theta)\mathcal{B}/128, & \text{for helicities } \{+ - + +\}, \{+ - - -\}, \{- + + +\}, \text{ and } \{- + - -\} \\ 3\beta^2\sin^6(\theta/2)\cos^2(\theta/2)\mathcal{B}/8, & \text{for helicities } \{+ - - +\} \text{ and } \{- + + -\} \\ 3\beta^2\sin^2(\theta/2)\cos^6(\theta/2)\mathcal{B}/8, & \text{for helicities } \{+ - + -\} \text{ and } \{- + - +\} \end{cases}, \tag{A6}$$

with

$$\mathcal{A} = \frac{s^2}{(s - m_{Z'}^2)^2 + m_{Z'}^2\Gamma_{Z'}^2}, \qquad \mathcal{B} = \frac{s^4}{(s - m_G^2)^2 + m_G^2\Gamma_G^2}, \tag{A7}$$

where θ is the polar angle between the momenta of the top quark and the light quark (or gluon) in the center of the mass frame of the top quark pair, s is the square of the center of mass energy, $\beta \equiv \sqrt{1 - 4m_{\text{top}}^2/s}$, and the squared amplitudes have been summed and averaged over the color of the external particles.

---

[1] C. T. Hill and E. H. Simmons, Phys. Rep. **381**, 235 (2003); **390**, 553(E) (2004).

[2] C. T. Hill, Phys. Lett. B **266**, 419 (1991); C. T. Hill and S. J. Parke, Phys. Rev. D **49**, 4454 (1994).

[3] N. Arkani-Hamed, A. G. Cohen, and H. Georgi, Phys. Lett. B **513**, 232 (2001); M. Schmaltz and D. Tucker-Smith, Annu. Rev. Nucl. Part. Sci. **55**, 229 (2005).

[4] P. Langacker, Rev. Mod. Phys. **81**, 1199 (2009).

[5] S. Godfrey and T. A. W. Martin, Phys. Rev. Lett. **101**, 151803 (2008).

[6] L. Randall and R. Sundrum, Phys. Rev. Lett. **83**, 3370 (1999).

[7] A. L. Fitzpatrick, J. Kaplan, L. Randall, and L. T. Wang, J. High Energy Phys. 09 (2007) 013.

[8] T. Gherghetta and A. Pomarol, Nucl. Phys **B586**, 141 (2000); B. Lillie, L. Randall, and L. T. Wang, J. High Energy Phys. 09 (2007) 074; B. Lillie, J. Shu, and T. M. P. Tait, Phys. Rev. D **76**, 115016 (2007); U. Baur and L. H. Orr, Phys. Rev. D **77**, 114001 (2008).

[9] K. Agashe et al., Phys. Rev. D **76**, 115015 (2007); A. Djouadi, G. Moreau, and R. K. Singh, Nucl. Phys. **B797**, 1 (2008).

[10] V. Barger, T. Han, and D. G. E. Walker, Phys. Rev. Lett. **100**, 031801 (2008).

[11] R. Frederix and F. Maltoni, J. High Energy Phys. 01 (2009) 047; Y. Bai and Z. Han, J. High Energy Phys. 04 (2009) 056.

[12] P. Mathews, V. Ravindran, and K. Sridhar, J. High Energy Phys. 10 (2005) 031.

[13] Q. Li, C. S. Li, and L. L. Yang, Phys. Rev. D **74**, 056002 (2006).

[14] G. L. Bayatian et al. (CMS Collaboration), J. Phys. G **34**, 995 (2007).

[15] C. Csaki, arXiv:hep-ph/0404096.

[16] T. Han, J. D. Lykken, and R. J. Zhang, Phys. Rev. D **59**, 105006 (1999).

[17] J. M. Campbell, R. K. Ellis, and F. Tramontano, Phys. Rev. D **70**, 094012 (2004); Q. H. Cao and C. P. Yuan, Phys. Rev. D **71**, 054022 (2005).

[18] G. 't Hooft and M. J. G. Veltman, Nucl. Phys. **B44**, 189 (1972).

[19] M. S. Chanowitz, M. Furman, and I. Hinchliffe, Nucl. Phys. **B159**, 225 (1979).

[20] B. W. Harris and J. F. Owens, Phys. Rev. D **65**, 094032 (2002).

[21] C. Amsler et al. (Particle Data Group), Phys. Lett. B **667**, 1 (2008).

[22] J. Pumplin, D. R. Stump, J. Huston, H. L. Lai, P. M.

Nadolsky, and W. K. Tung, J. High Energy Phys. 07 (**2002**) 012.

[23] J. C. Collins and D. E. Soper, Phys. Rev. D **16**, 2219 (1977).

[24] D. E. Kaplan, K. Rehermann, M. D. Schwartz, and B. Tweedie, Phys. Rev. Lett. **101**, 142001 (2008); J. Thaler and L. T. Wang, J. High Energy Phys. 07 (2008) 092; S. D. Ellis, C. K. Vermilion, and J. R. Walsh, Phys. Rev. D **80**,

051501 (2009); G. Giurgiu (for the CMS Collaboration), arXiv:0909.4894.

[25] A. D. Martin, R. G. Roberts, W. J. Stirling, and R. S. Thorne, Phys. Lett. B **604**, 61 (2004).

[26] A. D. Martin, W. J. Stirling, R. S. Thorne, and G. Watt, Eur. Phys. J. C **64**, 653 (2009).

[27] G. Mahlon, arXiv:hep-ph/0011349.